Role of the Conserved Acidic Residue Asp21 in the Structure of Phosphatidylinositol 3-Kinase Src Homology 3 Domain: Circular Dichroism and Nuclear Magnetic Resonance Studies†

Nobuyuki Okishio,*,‡ Toshiyuki Tanaka,*,§ Ryuji Fukuda,‡,⊥ and Masako Nagai||

Department of Biochemistry, School of Medicine, Kanazawa University Faculty of Medicine, Kanazawa, Ishikawa 920-8640, Japan, Institute of Applied Biochemistry and Center for Tsukuba Advanced Research Alliance, University of Tsukuba, Tsukuba, Ibaraki 305-8572, Japan, and School of Health Sciences, Kanazawa University Faculty of Medicine, Kanazawa, Ishikawa 920-0942, Japan

Received July 11, 2000; Revised Manuscript Received October 12, 2000

ABSTRACT: To elucidate a role of the Src homology 3 (SH3)-conserved acidic residue Asp21 of the phosphatidylinositol 3-kinase (PI3K) SH3 domain, structural changes induced by the D21N mutation (Asp21 → Asn) were examined by circular dichroism (CD) and nuclear magnetic resonance (NMR) spectroscopies. In the previous study, we demonstrated that environmental alterations occurred at the side chains of Trp55 and some Tyr residues from the comparison of the near-UV CD spectra of the PI3K SH3 domain with or without a D21N mutation [Okishio, N., et al. (2000) *Biopolymers 57*, 208−217]. In this work, the affected Tyr residues were identified as Tyr14 and Tyr73 by the CD analysis of a series of mutants, in which every single Tyr residue was replaced by a Phe residue with or without a D21N mutation. The ^{1}H and ^{15}N resonance assignments of the PI3K SH3 domain and its D21N mutant revealed that significant chemical shift changes occurred to the aromatic side-chain protons of Trp55 and Tyr14 upon the D21N mutation. All these aromatic residues are implicated in ligand recognition. In addition, the NMR analysis showed that the backbone conformations of Lys15−Asp23, Gly54−Trp55, Asn57−Gly58, and Gly67−Pro70 were affected by the D21N mutation. Furthermore, the ^{15}N{^{1}H} nuclear Overhauser effect values of Tyr14, Glu19, and Glu20 were remarkably changed by the mutation. These results show that the D21N mutation causes structural deformation of more than half of the ligand binding cleft of the domain and provide evidence that Asp21 plays an important role in forming a well-ordered ligand binding cleft in cooperation with the RT loop (Lys15-Glu20).

Src homology 3 (SH3)[1] domains, originally identified as homologous noncatalytic regions in the avian sarcoma viral protein p47$^{gag-crk}$ and bovine brain phospholipase C (*1*), are now known to be widely distributed among proteins involved in intracellular signaling and cytoskeletal organization. Numerous studies have shown that SH3 domains interact with proline-rich sequences and mediate specific protein−protein interactions (*2*).

The class IA phosphatidylinositol 3-kinase (PI3K) is a heterodimeric enzyme composed of a noncatalytic 85 kDa (p85) subunit and a catalytic 110 kDa (p110) subunit that contains PI3K and serine kinase activities. The noncatalytic subunit has several functional domains: an SH3 domain, a breakpoint cluster region homology domain, two proline-rich regions, and two Src homology 2 domains. This points out that the p85 subunit may have multiple interactive and regulatory roles (*3, 4*). Several proteins have been identified to interact with the p85 SH3 domain (the PI3K SH3 domain). The GTPase activity of dynamin is stimulated by binding to this domain (*5*). CDC42 GTPase-activating protein (*6*) and an adapter protein Shc (*7*) can also be associated with the SH3 domain. The overexpression of the PI3K SH3 domain reverts v−Ha−Ras transformation activity (*8*). The SH3 domain also takes a part in the dimerization of the p85 subunit (*9*). These facts denote the importance of the PI3K SH3 domain in signal transduction pathways and cytoskeletal interactions. In addition to biochemical characterization, the three-dimensional (3D) structures of the PI3K SH3 domain have been determined by nuclear magnetic resonance (NMR) spectroscopy with or without a ligand peptide RLP1 (RKLP-PRPSK) (*10*−*12*) and X-ray crystallography (*13*).

Despite the diversity of amino acid sequences, SH3 domains share a very similar tertiary structure and a binding

† This work was supported by a Grant-in-Aid for Scientific Research to M.N. (11116209) from the Ministry of Education, Science, Sports and Culture of Japan and a "Research for the Future" Program to T.T. (96L00501) from the Japan Society for the Promotion of Science.

* To whom correspondence should be addressed. For N.O.: telephone, 81 76 265 2176; fax, 81 76 234 4225; e-mail, okishio@med.kanazawa-u.ac.jp. For T.T.: telephone and fax, 81 298 53 6706 or 81 298 53 6065; e-mail, ttanaka@tara.tsukuba.ac.jp.

‡ Department of Biochemistry, Kanazawa University.

⊥ E-mail: rfukuda@med.kanazawa-u.ac.jp.

§ University of Tsukuba.

|| School of Health Sciences, Kanazawa University. Telephone: 81 76 265 2581. Fax: 81 76 234 4360. E-mail: nagai@kenroku.kanazawa-u.ac.jp.

[1] Abbreviations: CD, circular dichroism; COSY, correlated spectroscopy; HIV-I, human immunodeficiency virus type I.; HSQC, heteronuclear single-quantum correlation; K_d, dissociation constant; NMR, nuclear magnetic resonance; NOE, nuclear Overhauser effect; NOESY, nuclear Overhauser effect spectroscopy; PI3K, phosphatidylinositol 3-kinase; SH3, Src homology 3; UVRR, UV resonance Raman; 2D, two-dimensional; 3D, three-dimensional.

10.1021/bi001607v CCC: $20.00
Published on Web 12/13/2000

mode to ligand peptides. These peptides have a consensus sequence of PxxP and adopt a left-handed polyproline type II helix conformation when bound to the domain (*14*). The SH3−ligand association is partly contributed by hydrophobic interactions between the conserved hydrophobic residues of the SH3 domain and the PxxP region of the binding peptide and often reinforced by electrostatic interactions between the conserved acidic residue in the SH3 domain (Asp21 in PI3K SH3) and the basic residue positioned before or after the PxxP motif of the ligand peptide (Arg1 in RLP1) (*14*). This acidic residue is placed next to the RT loop (Lys15−Glu20 in PI3K SH3), whose amino acid sequences and structures are rich in variety among SH3 domains and uniquely conserved in this region of the SH3 family. The role of the acidic residue has been mainly thought to be related to the SH3−ligand interaction, but it is also suggested that this residue may be necessary for forming a well-ordered ligand binding cleft of the SH3 domain (*15*−*17*). For instance, Yu et al. (*12*) found that the D21N mutation (Asp21 → Asn) of PI3K SH3 profoundly decreased the binding affinity for the RLP1 peptide by about 50-fold, while the affinity of the wild-type PI3K SH3 for the mutated RLP1 (Ala for Arg1, R1A mutant) was only moderately decreased by about 10-fold. One possible explanation for this difference is that the D21N mutation may cause severe structural deformation of the binding cleft of the SH3 domain; however, it has not been clarified yet.

Thus, in this study, we compared the structure of the wild-type PI3K SH3 domain with that of the D21N mutant by circular dichroism (CD) and NMR spectroscopies and revealed that the D21N mutation caused structural alterations in the ligand binding site. These data provide evidence for another important role of the conserved acidic residue of the SH3 domain.

MATERIALS AND METHODS

Sample Preparation. The recombinant PI3K SH3 and its D21N mutant proteins were prepared as described previously (*17*). Substitution of a phenylalanine or a histidine for a tyrosine residue was introduced by PCR-mediated site-directed mutagenesis. Introduced mutations are Y6F, tac(Tyr6) → ttc(Phe); Y8F, tac(Tyr8) → ttc(Phe); Y12F, tat(Tyr12) → ttc(Phe); Y14F, tat(Tyr14) → ttc(Phe); Y59F, tat(Tyr59) → ttc(Phe); Y73F, tac(Tyr73) → ttc(Phe); Y76F, tat(Tyr76) → ttt(Phe); Y14H, tat(Tyr14) → cac(His). The subcloned fragments were sequenced to confirm the absence of unintentional mutations. These mutant proteins were expressed and purified in the similar way with the wild-type protein (*17*). The recombinant SH3 domain or its mutants consist of 90 residues, 85 residues from the domain and additional N-terminal 5 residues (GPLGS) from a vector sequence. The concentration of proteins was determined by absorbance at 280 nm. The extinction coefficient of the protein denatured in 6 M guanidine hydrochloride solution was calculated according to the method of Gill and von Hippel (*18*). The values are 14 650 M^{-1} cm^{-1} for the wild type and the D21N mutant and 13 370 M^{-1} cm^{-1} for the Phe- or His-substituted mutants.

CD Measurements and Determination of Dissociation Constant Values. All CD spectra were recorded on a Jasco J-725 spectropolarimeter at 25 °C. The instrument was calibrated with *d*-10-camphorsulfonic acid. Determination of the dissociation constant (K_d) values of the PI3K SH3 domain and its Y → F (Tyr → Phe) or Y14H mutants for the ligand peptide RLP1 (RKLPPRPSK−NH_2) (*12*, *17*) was performed by monitoring the alterations of CD intensity in the 280−310 nm region with increasing peptide concentration (*19*, *20*) as follows: Aliquots of a concentrated peptide solution (10 mM) were added to a 2 mL solution of the domain (10 μM) in phosphate-buffered saline (pH 7.4). The mixture was incubated at 25 °C in a stirred cell for 5−10 min before CD measurements. CD spectra were acquired for a light path of 1 cm at a scan speed of 100 nm min^{-1} with a 2 nm slit width and 1 s response time, and 50 scans were averaged. The raw CD data were corrected for protein dilution. The concentration of the free RLP1 peptide was calculated by subtracting the concentration of the SH3−RLP1 complex, which was estimated by the CD change, from the concentration of the added peptide. The highest difference peak in the near-UV region between with and without RLP1 was used to monitor CD changes: a peak at 291 nm for the Y73F, 284 nm for the Y14H, and 285 nm for the wild type and the other Y → F mutants. The added peptide contains no aromatic and Cys residues and hence exhibits no CD signal in the near-UV region (*17*). K_d values were calculated by Scatchard analysis using the following equation where $\Delta\theta$ is the difference between the observed CD intensity and the CD intensity of the SH3 domain without the ligand, $\Delta\theta_\infty$ denotes the difference between the CD intensity of the completely liganded SH3 domain and the CD intensity of the SH3 domain without the ligand, [L] is the concentration of the free RLP1 peptide, and n is the number of binding sites.

$$(\Delta\theta/\Delta\theta_\infty)/[\mathrm{L}] = n/K_d - (\Delta\theta/\Delta\theta_\infty)/K_d$$

Other CD spectra were acquired at the same condition as that used in the previous study (*17*): Sample concentration was 0.05 or 0.2 mM in 50 mM Tris-HCl (pH 7.2) containing 0.1 M sodium sulfate for a light path of 1 mm at a scan speed of 50 nm min^{-1} with a 1 nm slit width and 1 s response time, and 20 scans were averaged. CD data were expressed in terms of mean residue molar ellipticity (θ) (deg cm^2 $dmol^{-1}$). In the previous study, sodium sulfate was used for an internal intensity standard in UV resonance Raman (UVRR) spectroscopy and, therefore, added to the CD samples to compare directly UVRR and CD data.

NMR Spectroscopy. Uniformly ^{15}N-labeled protein was obtained by growing cells in M9 minimal medium that contained $^{15}NH_4Cl$ (Isotech, Miamisburg, OH) as the sole nitrogen source. Samples for NMR experiments were prepared by exchanging a buffer solution to a 90% H_2O/10% D_2O (v/v) or a 95% H_2O/5% D_2O (v/v) solution containing 50 mM potassium phosphate and 100 mM potassium chloride (pH 6.0). Protein concentrations were in the range of 1.0−2.0 mM. NMR experiments were performed on a Varian UNITY INOVA 500 spectrometer at 25 °C. All data were processed using the software NMRPipe and NMRDraw (*21*), and the data analysis was assisted by the software Capp and Pipp (*22*).

Homonuclear two-dimensional (2D) correlated spectroscopy (COSY) (*23*) and nuclear Overhauser effect spectroscopy (NOESY) (*24*) spectra were recorded with the following numbers of complex points and acquisition times: ^1H (F_1)

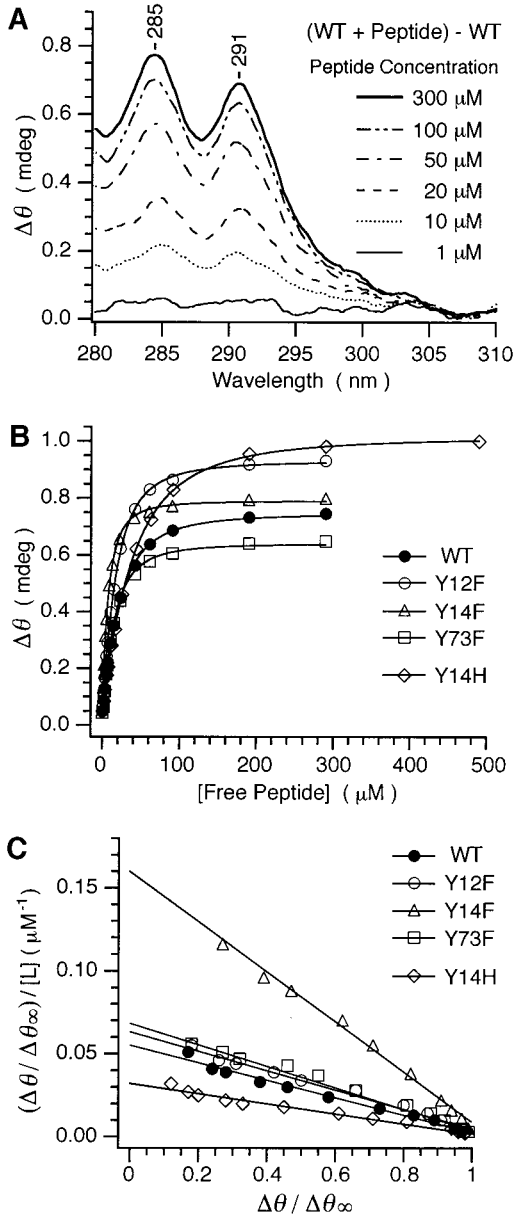

FIGURE 1: Representative data for the binding assay of the PI3K SH3 domain and its mutants for the RLP1 peptide. (A) Effect of the RLP1 binding on the near-UV CD difference spectra of the wild-type PI3K SH3 domain (WT). The difference spectra of the wild type between with and without RLP1 at various peptide concentrations are shown. (B) Titration curves of the CD differences ($\Delta\theta$) of the PI3K SH3 domain and its Y12F, Y14F, Y73F, and Y14H mutants. The CD difference between with and without RLP1 was plotted against the calculated concentration of the free RLP1 peptide. (C) Scatchard analysis of the PI3K SH3 domain and its Y12F, Y14F, Y73F, and Y14H mutants. The K_d value was calculated from the slope of the plot. The values of slope, the coefficients of determination (r^2), and the numbers of binding sites (n) are summarized in Table 3 of Supporting Information.

512, 64 ms; ^{1}H (F_2) 512, 64 ms (32 transients). For the NOESY experiment, a mixing time of 200 ms was used.

A 2D ^{1}H−^{15}N heteronuclear single-quantum correlation (HSQC) (*25*) spectrum was recorded with the following numbers of complex points and acquisition times: ^{15}N (F_1) 256, 128 ms; ^{1}H (F_2) 512, 51 ms (64 transients). A 3D ^{15}N-edited NOESY−HSQC (*25*, *26*) spectrum was recorded with a mixing time of 100 ms. The following numbers of complex points and acquisition times were used: ^{1}H (F_1) 128, 21 ms; ^{15}N (F_2) 32, 16 ms; ^{1}H (F_3) 1024, 102 ms (16 transients).

Table 1: Dissociation Constants of the Wild-Type PI3K SH3 Domain and Its Mutants for the RLP1 Peptide

SH3 domain	K_d (μM)	SH3 domain	K_d (μM)
wild type	19	Y59F	20
Y6F	20	Y73F	16
Y8F	20	Y76F	19
Y12F	17	Y14H	33
Y14F	7		

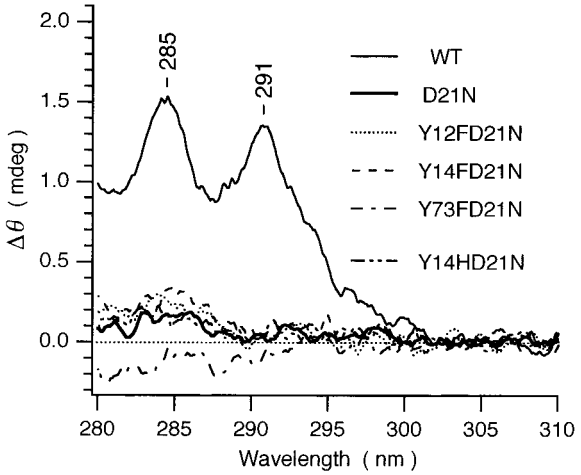

FIGURE 2: Near-UV CD difference spectra of the wild-type PI3K SH3 domain and its D21N, Y12FD21N, Y14FD21N, Y73FD21N, and Y14HD21N mutants between with and without RLP1. The sample concentration was 0.2 mM SH3 domain in 50 mM Tris-HCl (pH 7.2) containing 0.1 M sodium sulfate with or without 0.8 mM RLP1.

The ^{15}N{^{1}H} nuclear Overhauser effect (NOE) was measured as described (*27*). Three sets of spectra with and without the NOE effect were recorded with the following numbers of complex points and acquisition times: ^{15}N (F_1) 256, 128 ms; ^{1}H (F_2) 1024, 102 ms (32 transients). Resonance intensities were used to determine the NOE values, and the average values of three experiments were calculated.

RESULTS

Determination of the K_d Values of the PI3K SH3 Domain and Its Y → F or Y14H Mutants for the Ligand Peptide RLP1. To identify the specific Tyr residues affected by the D21N mutation, we constructed a series of mutants in which every single Tyr residue was replaced by a Phe residue with or without a D21N mutation. For Tyr14, a His-substituted mutant with or without a D21N mutation was also made. At first, we compared the binding affinities of the wild-type PI3K SH3 domain and its Y → F or Y14H mutants for the ligand peptide RLP1. Representative data for the binding assay are shown in Figure 1. On the addition of the RLP1 peptide to the wild-type SH3, the CD intensity in the near-UV region increased with peptide concentration (Figure 1A), and these CD changes allowed us to determine the K_d value. The CD difference ($\Delta\theta$) at 285 nm of the wild type between with and without RLP1 was plotted against the concentration of the free RLP1 peptide (Figure 1B), and its Scatchard analysis (Figure 1C) gave a K_d value of 19 μM. The K_d values of the mutants were obtained similarly (Figure 1B,C) and are summarized in Table 1. The values of the Y → F mutants

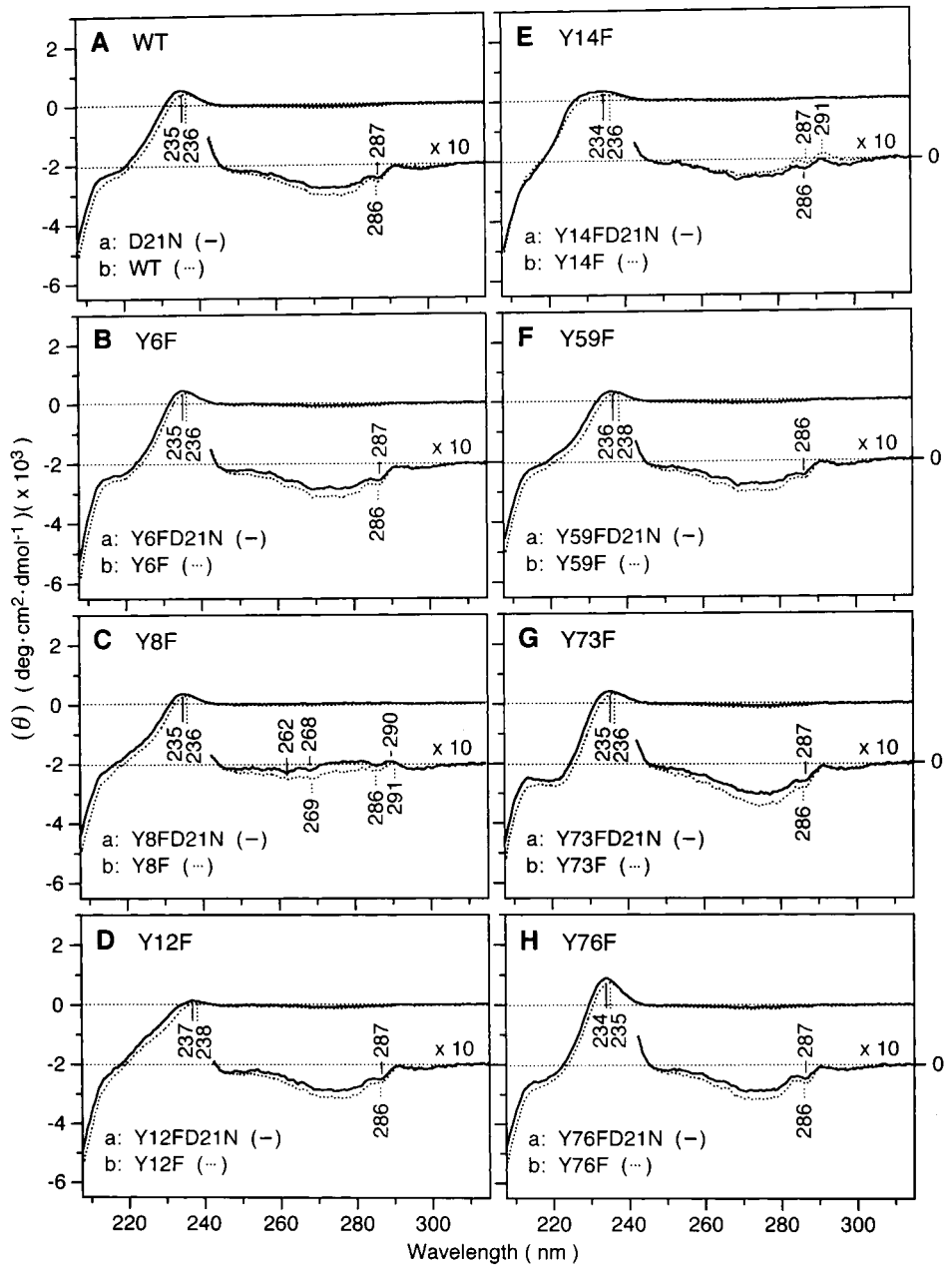

FIGURE 3: Comparison of the UV CD spectra of the PI3K SH3 domain and its Y → F mutants between with (solid line) and without (dotted line) a D21N mutation: (A) wild type (D21N and WT); (B) Y6F mutant (Y6FD21N and Y6F); (C) Y8F mutant (Y8FD21N and Y8F); (D) Y12F mutant (Y12FD21N and Y12F); (E) Y14F mutant (Y14FD21N and Y14F); (F) Y59F mutant (Y59FD21N and Y59F); (G) Y73F mutant (Y73FD21N and Y73F); (H) Y76F mutant (Y76FD21N and Y76F). The protein concentration was 0.05 mM (0.2 mM for 10-fold expanded spectra) in 50 mM Tris-HCl buffer (pH 7.2) containing 0.1 M sodium sulfate.

of Tyr6, Tyr8, Tyr59, and Tyr76 (19−20 μM), which are all located far from the ligand binding cleft, were similar to that of the wild type (19 μM). In contrast, the K_d values of the Y → F mutants of Tyr12, Tyr14, and Tyr73, which constitute the ligand binding cleft, decreased to 17, 7, and 16 μM, respectively. In the case of the Y14H mutant, the K_d value increased to 33 μM. As a whole, the introduced mutations did not change the K_d values significantly.

Introducing the D21N mutation to these Y → F or Y14H mutants brought about drastic effects on their affinities for the RLP1 peptide. The CD difference spectra between with and without RLP1 of the Y12F, Y14F, Y73F, and Y14H mutants with a D21N mutation are shown in Figure 2. For these double mutants, addition of RLP1 hardly induced CD spectral changes in the near-UV region even in the condition of 200 μM SH3 with 800 μM RLP1, as was observed for the D21N mutant. Similar results were obtained for the double mutants of D21N with Y6F, Y8F, Y59F, and Y76F (data not shown). These results indicate that the binding affinities for the ligand decrease severely and that the feature of the D21N mutant in ligand affinity is preserved in the Y → F or Y14H mutants with a D21N mutation.

CD Analysis of the PI3K SH3 Domain and Its Y → F or Y14H Mutants. Figure 3 shows the UV CD spectra of the wild type and Y → F mutants of the PI3K SH3 domain with or without a D21N mutation. The spectral changes induced by the mutation were clearly observed in the difference spectra between with and without a D21N mutation as shown in Figure 4. Since there is no Cys residue in PI3K SH3, CD changes in the near-UV region are attributed to alterations

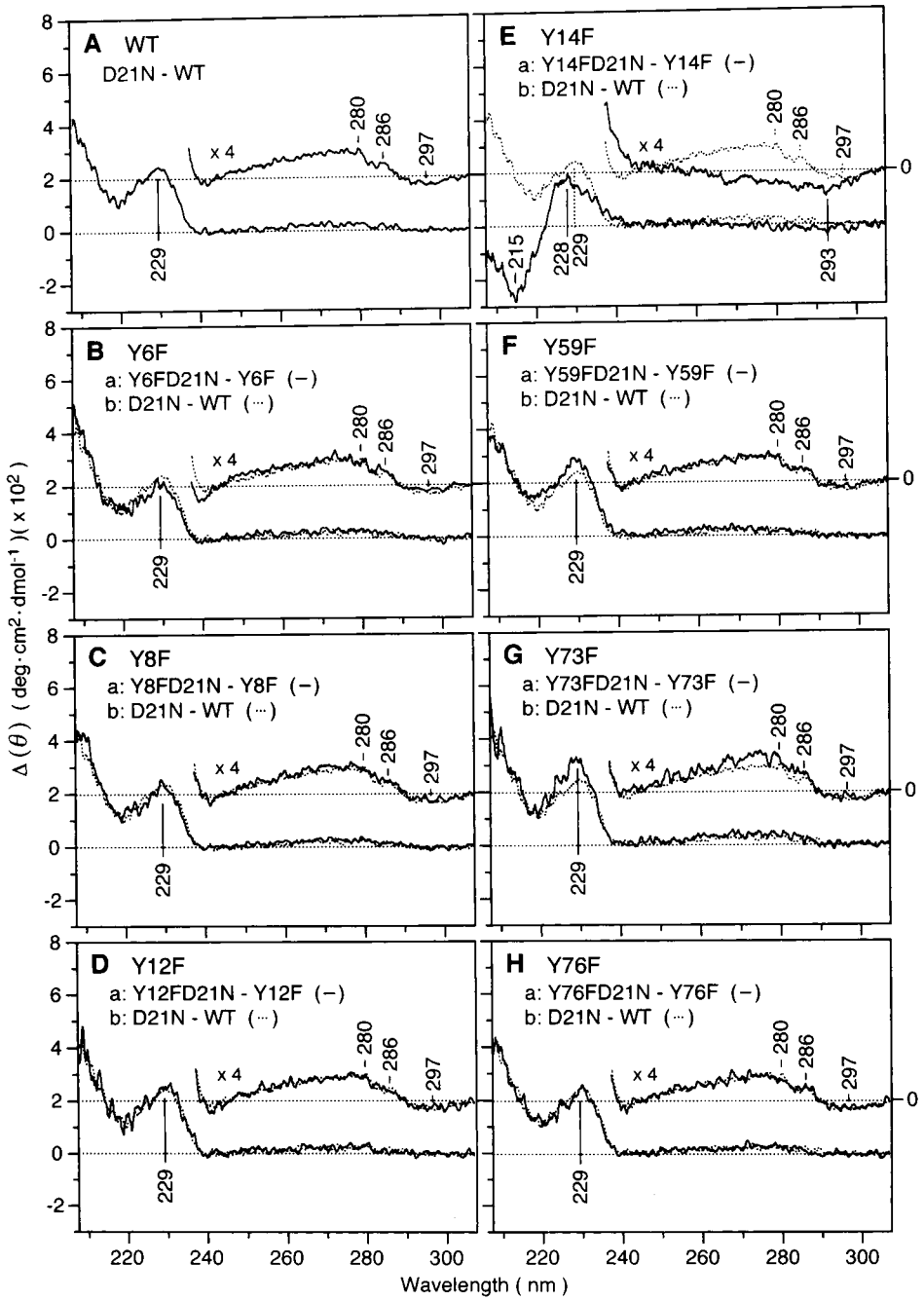

FIGURE 4: UV CD difference spectra of the PI3K SH3 domain and its Y → F mutants between with and without a D21N mutation: (A) wild type (D21N − WT); (B) Y6F mutant (Y6FD21N − Y6F); (C) Y8F mutant (Y8FD21N − Y8F); (D) Y12F mutant (Y12FD21N − Y12F); (E) Y14F mutant (Y14FD21N − Y14F); (F) Y59F mutant (Y59FD21N − Y59F); (G) Y73F mutant (Y73FD21N − Y73F); (H) Y76F mutant (Y76FD21N − Y76F). The difference spectra are shown in a solid line. The difference spectra of the wild type (A) are drawn in a dotted line in panels B−H for comparison.

in the surroundings of aromatic side chains (*28*, *29*). The difference spectrum between the D21N mutant and the wild type showed peaks at 297, 286, 280, and 229 nm with a broad positive band in the 280−240 nm region (Figure 4A). Each of aromatic amino acids is known to have a characteristic wavelength profile of CD: Trp, a peak close to 290 nm with a fine structure between 290 and 305 nm; Tyr, a peak between 275 and 282 nm (the fine structure at longer wavelength may be obscured by that of Trp); Phe, a sharp fine structure between 255 and 270 nm (*19*). Consequently, it is considered that the negative peak at 297 nm originates from Trp55, a unique Trp residue in the SH3 domain, and that the two positive peaks at 286 and 280 nm with a broad positive band in 280−240 nm are mainly from some Tyr residues. In the Y → F mutants, the Y6F, Y8F, Y12F, Y59F, and Y76F mutants showed very similar difference spectra with that of the wild type in both of the near- and far-UV regions (parts B, C, D, F, and H of Figure 4, respectively). In contrast, significant differences were observed in the Y14F mutant (Figure 4E). The difference spectrum showed a broad and increased negative band with a peak at 293 nm in the near-UV region along with positive and negative peaks at 228 and 215 nm, respectively, in the far-UV region. In the Y73F mutant, small increments of the difference spectrum were observed at around 260−280 and 229 nm (Figure 4G).

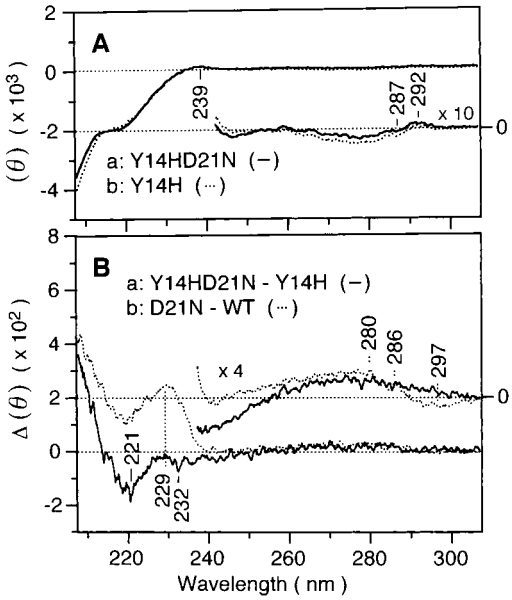

FIGURE 5: UV CD spectra of the Y14H mutant with and without a D21N mutation (A) and the difference spectra between them (B). (A) The spectra of the Y14H mutant with and without a D21N mutation are drawn in a solid and dotted line, respectively. (B) The difference spectra between Y14HD21N and Y14H are drawn in a solid line. The difference spectra between the D21N mutant and the wild type (Figure 4A) are shown in a dotted line for comparison. Experimental conditions are the same as those in Figure 3.

Interested in the alteration of CD spectra of the Y14F mutant upon the D21N mutation (Figure 4E), we measured the UV CD spectra of the Y14H mutant with and without a D21N mutation (Figure 5). Histidine was selected for the substitution because its side chain has a ring structure of a similar size with tyrosine and phenylalanine but with more hydrophilic character than them. The difference spectrum of the Y14H mutant (Figure 5B) was dissimilar to those of the wild type (Figure 4A) and the Y14F mutant (Figure 4E), exhibiting a broad positive band in the near-UV region along with small and large negative peaks at 232 and 221 nm, respectively, in the far-UV region. Distinguishable appearances of the difference spectra around 290−305 nm between the wild type and the Y14F mutant (Figure 4E) and between the wild type and the Y14H mutant (Figure 5B) should be noted. These can exist because of the different environmental changes that were induced to Trp55 upon the D21N mutation among them.

NMR Analyses of the PI3K SH3 Domain and Its D21N Mutant. NMR analyses were applied to investigate the backbone structural changes induced by the D21N mutation. The 2D $^{1}H-^{15}N$ HSQC spectra of the wild type and the D21N mutant of PI3K SH3 are overlaid in Figure 6. Their ^{1}H and ^{15}N resonances were assigned by analyzing homonuclear 2D COSY (*23*) and NOESY (*24*) and 3D ^{15}N-edited NOESY−HSQC (*25*, *26*) spectra. For both of the proteins, all of the amide ^{15}N resonances and more than 87% of the ^{1}H resonances were assigned from Ala3 to Ser83. The obtained assignments of the wild-type PI3K SH3 domain were basically coincident with those reported by Koyama et al. (*30*), although our recombinant protein contained extra N-terminal 5 residues from a vector sequence. In Figure 7, the chemical shift differences of backbone NH (Figure 7A) and $C_{\alpha}H$ (Figure 7B) between the D21N mutant and the wild type are shown. The NH chemical shifts of Lys15−Asp23, Trp55, Asn57, Gly58, and Gly67−Phe69 as well as the $C_{\alpha}H$ chemical shifts of Glu17−Asp21, Gly54, Trp55, Asn57, and Asp68−Pro70 were significantly perturbed (±0.05 ppm or more) when the D21N mutation was introduced. Accordingly, the backbone structures of Lys15−Asp23, Gly54−Trp55, Asn57−Gly58, and Gly67−Pro70 are likely to be affected by the D21N mutation. Quite small (<±0.05 ppm) chemical shift differences of the other backbone protons denote that the effect of the D21N mutation is localized to the part of the domain and that the overall structure is hardly deformed. The strong changes of NH chemical shifts of the residues in the RT loop, especially Glu17 (−1.6 ppm) and Arg18 (−0.9 ppm), should be noted.

To make a comparison with the results of CD analysis, the influence of the D21N mutation on aromatic side chains was analyzed by NMR spectroscopy. The aromatic region of 2D NOESY spectra of the wild type and the D21N mutant is depicted in Figure 8 (also see Tables 1 and 2 of Supporting Information for the chemical shift differences of aromatic side-chain protons). The H_{ϵ} of Tyr14 and all of the aromatic protons of Trp55 except $H_{\epsilon 1}$ showed a strong proton chemical shift difference of ±0.05 ppm or more between with and without a D21N mutation. The H_{δ} of Tyr14 and the $H_{\epsilon 1}$ of Trp55 along with the H_{δ} and H_{ϵ} of Tyr73 showed a smaller difference of ±0.03 ppm. The other aromatic residues were hardly affected by the D21N mutation. The affected aromatic side chains assigned by NMR spectroscopy are coincident with those by CD analysis (Figure 4).

In addition to static information, effects of the D21N mutation to intrinsic dynamics of the SH3 domain were evaluated by $^{15}N\{^{1}H\}$ NOE measurements (*27*). Figure 9 shows the $^{15}N\{^{1}H\}$ NOE values of each residue of the wild type and the D21N mutant of PI3K SH3. As for the wild type, N- and C-terminal regions, Arg18−Glu20, and Val38−Gly45 showed NOE values of 0.7 or less, indicating that these regions have a higher degree of conformational flexibility compared with the other regions. Similar tendency was observed for the D21N mutant, but the NOE values of Tyr14, Glu19, and Glu20 increased significantly.

DISCUSSION

In the previous study, we showed that the surroundings of the Trp and Tyr residues of the PI3K SH3 domain were perturbed by the D21N mutation from the comparison of the near-UV CD spectra of the SH3 domain with or without the mutation (*17*). Trp55 was determined to be involved in the structural changes from the negative difference peak at 297 nm (*17*). However, Tyr residues affected by the D21N mutation could not be assigned because there are seven Tyr residues in the SH3 domain. Therefore, we constructed a series of mutants, in which every single Tyr residue was replaced by a phenylalanine with or without a D21N mutation, to assign the affected Tyr residues.

Phe-substitution for any Tyr residues in the ligand binding cleft of the PI3K SH3 domain (Tyr12, Tyr14, and Tyr73) caused some increments of the binding affinity for the RLP1 peptide (Table 1). Substitution of Phe for Tyr may increase the hydrophobicity of the binding cleft and subsequently the affinity for the ligand. The effect of Phe-substitution was most prominent in the Y14F mutant. Tyr14 is known to be

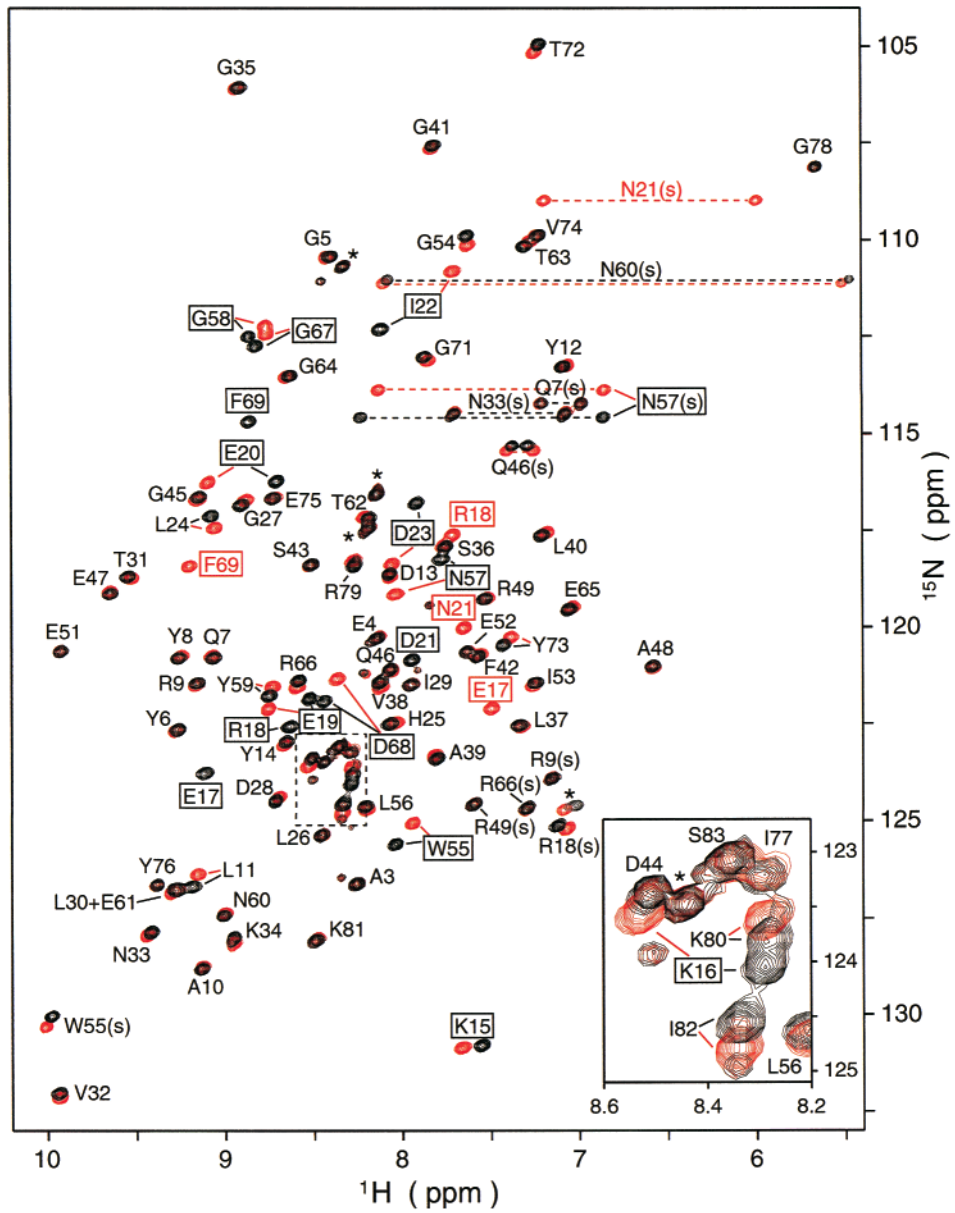

FIGURE 6: Two-dimensional ^{1}H-^{15}N HSQC spectra of the wild type (black) and the D21N mutant (red). Backbone or side-chain cross-peaks whose amide proton chemical shifts change by ±0.05 ppm or more upon the D21N mutation are indicated by rectangles. The inset shows the expanded view of the region enclosed by a dotted line. Cross-peaks connected by dotted lines correspond to Asn or Gln side-chain NH_2 groups. Unassigned and side-chain cross-peaks are labeled with an asterisk and (s), respectively.

in contact with Pro4 of the RLP1 peptide (*12*). Thus, increased hydrophobic interaction between Phe14 of the Y14F mutant and Pro4 of the RLP1 peptide may cause the increment of the affinity. This is consistent with the observation that the binding affinity decreased in the Y14H mutant where more hydrophilic substitution was introduced (Table 1). Differences in size, hydrophobicity, and functional group of the aromatic side chains in the ligand binding cleft may increase the diversity in ligand specificity and/or affinity of SH3 domains. The use of Phe or His for the Tyr residues in the ligand binding cleft is indeed seen in some other SH3 domains such as Abl, α-Spectrin, Crk, and Grb2/Sem5 (*14*). Furthermore, it has been shown that the Eps8 SH3 domain, which has an isoleucine residue at the position corresponding to Tyr73 of PI3K SH3, prefers the unusual PXXDY motif, and the Ile to Tyr mutation increases the affinity for PXXDY peptides more than 10-fold (*31*). This observation indicates that some SH3 domains do use other hydrophobic residues at the position where Tyr is predominant in other SH3 domains, even though higher affinity for a ligand is obtained when an aromatic residue is used.

As shown in Table 1, the effects of the Y → F and Y14H mutations on the binding affinity are relatively small, which suggests that the overall structure of the PI3K SH3 domain is hardly deformed by Phe- or His-substitution for a Tyr residue. Thus, the double mutants of D21N with Y → F or Y14H are expected to sustain the feature of the single D21N mutant. In fact, the CD spectral changes of the double mutants induced by RLP1 were profoundly decreased as was observed in the D21N mutant (Figure 2). This indicates that the affinities of the double mutants for RLP1 were lowered to the same extent as that of the single D21N mutant. Therefore, we compared the CD spectra of the wild type and the Y → F or Y14H mutants with and without a D21N mutation in order to assign Tyr residues responsible for the spectral changes induced by the D21N mutation. As shown

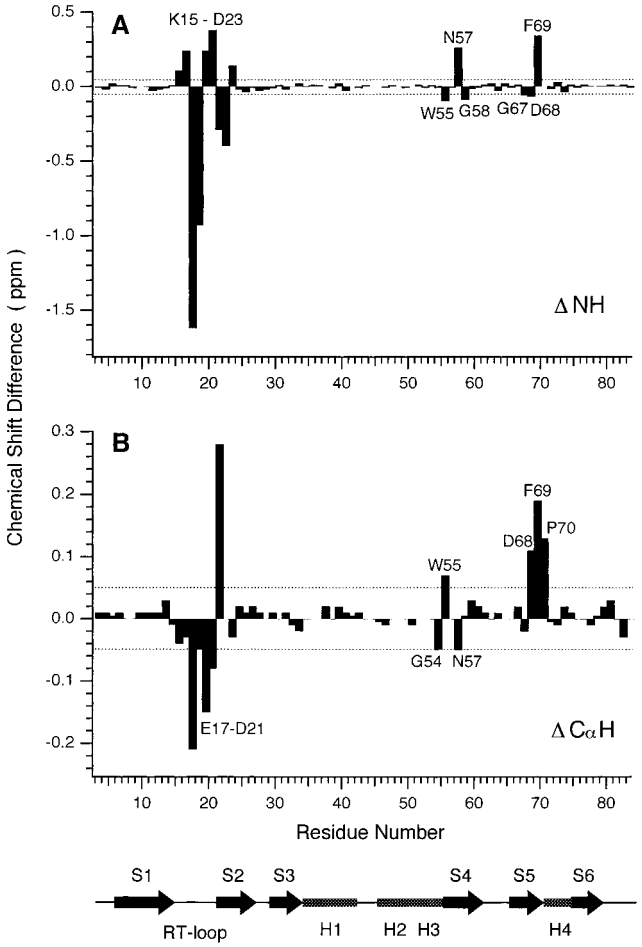

FIGURE 7: Chemical shift changes of backbone NH (A) and $C_\alpha H$ (B) of the PI3K SH3 domain by introducing the D21N mutation. The chemical shift values of the wild type were subtracted from those of the D21N mutant. At the bottom, cartoon representation of the secondary structure of the wild-type PI3K SH3, elucidated by Koyama et al. (*10*), is shown; β-strands are represented by arrows with labeling S1−S6 and α- or 3_{10}-helices by boxes with labeling H1−H4. The position of the RT loop is also indicated.

in Figure 4, only the Y14F mutant showed a significantly different appearance from the wild type in the near-UV region, pointing out the close relationships among Asp21, Tyr14, and Trp55. This is reinforced by the CD analysis of the Y14H mutant (Figure 5). These three residues are highly conserved among SH3 domains and constitute the ligand binding cleft of the domain. This observation suggests that the mutation of one of these residues affects the environments of the other residues and consequently brings about the structural changes of the ligand binding cleft and alters the ligand affinity and/or specificity. The environmental changes of the aromatic side chains of Tyr14 and Trp55 were also detected by NMR spectroscopy when the D21N mutation was introduced (Figure 8).

In addition to the aromatic side chains, the peptide backbone structure of the PI3K SH3 domain was altered by the D21N mutation. The main chains affected by the D21N mutation (Lys15−Asp23, Gly54−Gly58 except Leu56, and Gly67−Pro70) are highlighted in the schematic drawing of the C_α backbone trace of the wild-type PI3K SH3 domain (Figure 10A). The effect of the D21N mutation was localized around the RT loop and a part of the ligand binding cleft. The O_δ atoms of Asp21 are located within a distance of about

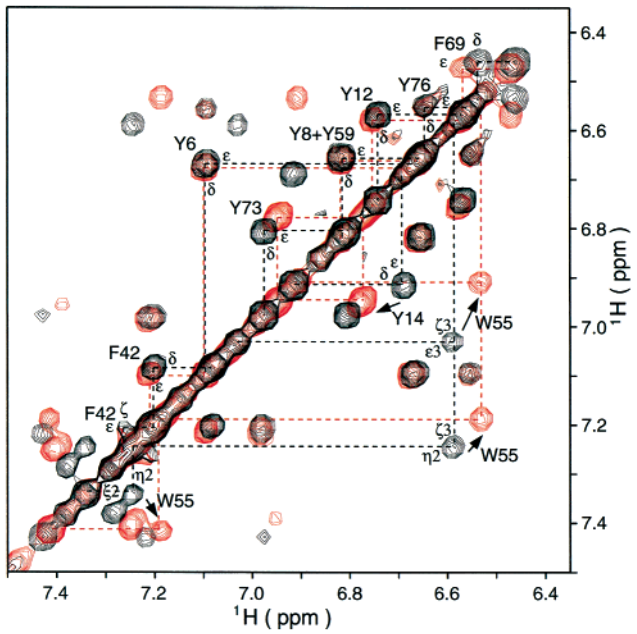

FIGURE 8: The aromatic region of 2D NOESY spectra of the wild type (black) and the D21N mutant (red). Only intraresidual cross-peaks of aromatic side chains are labeled. The cross-peaks of Tyr14 and Tyr73 in the D21N mutant overlap with each other.

3 Å from the O_η atom of Tyr14 or the N atoms of Glu17 and Arg18 (*10*), which indicates that they may form a network of hydrogen bonds. As illustrated in Figure 10B, the D21N mutation may break an interaction between Asp21 and Tyr14 (Tyr14 destabilized) or disrupt an association between Asp21 and Glu17 or Arg18 (RT loop deformed). The latter case is more plausible, because a notable difference in hydrogen-bonding state of a Tyr residue was not detected between the wild type and the D21N mutant by UVRR spectroscopy, which is sensitive to formation or loss of a hydrogen bond of a Tyr residue (*17*). Also, the significant decrements of NH chemical shift values of Glu17 and Arg18 (−1.6 and −0.9 ppm, respectively) by introducing the D21N mutation (Figure 7A) imply that the hydrogen bonds between their amide protons and the O_δ atoms of Asp21 are disrupted in the D21N mutant. The breakage of these hydrogen bonds may strengthen the remaining hydrogen bond between Asn-(Asp)21 and Tyr14 followed by the change in environment and the reduction of conformational flexibility of Tyr14, which were actually detected by the CD analysis (Figure 4) and the $^{15}N\{^1H\}$ NOE experiment (Figure 9), respectively. From these observations, it is reasonable to consider that the RT loop is deformed in the D21N mutant.

In the study on the interaction of the Hck SH3 domain with the Nef protein of human immunodeficiency virus type I (HIV-I), Arold et al. (*32*) observed that His97 and His98 of Hck SH3 (which correspond to Arg18 and Glu19 of PI3K SH3, respectively) were highly mobile and suggested that the flexibility of the RT loop might enhance the affinity to HIV-I Nef. In the D21N mutant of PI3K SH3, the decrements in mobility of Glu19 and Glu20 backbones were observed (Figure 9). The lower flexibility might be an additional cause of the decrement of the affinity for a ligand by the D21N mutation.

Regarding that Asp21 is highly conserved among SH3 domains, formation of a hydrogen bond with the residues in the RT loop seems to be one of the important roles of this

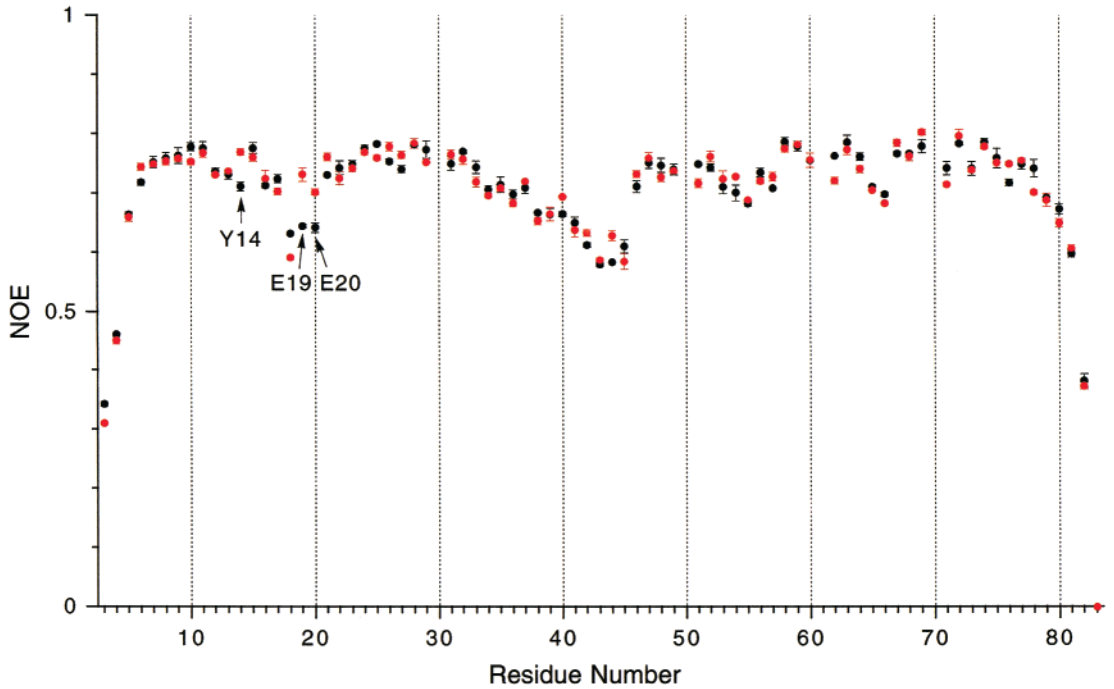

FIGURE 9: $^{15}N\{^{1}H\}$ NOE values of the PI3K SH3 domain (black) and the D21N mutant (red). The residues whose NOE values change by ±0.05 ppm or more upon the D21N mutation are labeled. For Leu30 and Glu61, the NOE values could not be estimated due to resonance overlap.

Table 2: Distances between the Two Closest Atoms Corresponding to Glu17N and Asp21Oδ of PI3K SH3 in Various SH3 Domains[a]

SH3 domain[b]		method	atom	distance (Å)
α-Spectrin	(1SHG)	X-ray	Lys18N−Glu22Oϵ	2.7
Abl	(1ABQ)	X-ray	Ser75N−Thr79Oγ	3.0
Amphiphysin 2	(1BB9)	X-ray	Thr35N−Glu39Oϵ	2.9
Btk	(1AWX)	NMR	Met20N−Asp24Oδ	4.3
Crk	(1CKA)	X-ray	Asn146N−Asp150Oδ	3.3
Csk	(1CSK)	X-ray	Thr23N−Asp27Oδ	2.7
Eps8	(1AOJ)	X-ray	Arg18N−Glu22Oϵ	2.8
Grb2 (N-terminal)	(3GBQ)	NMR	Thr12N−Glu16Oϵ	3.0
Grb2 (C-terminal)	(1GFC)	NMR	Gln14N−Glu18Oϵ	2.4
Hck	(5HCK)	NMR	Ile92N−Asp96Oδ	2.6
Lck	(1LCK)	X-ray	Ser75N−Asp79Oδ	3.1
Nebulin	(1NEB)	NMR	Ala15N−Glu19Oϵ	4.1
Sem5	(1SEM)	X-ray	Gln168N−Glu172Oϵ	2.8
Fyn	(1SHF)	X-ray	Arg96N−Asp100Oδ	2.7
	(1NYF)	NMR	Arg96N−Asp100Oδ	4.9
Itk	(1AWJ)	NMR	Asn34N−Glu38Oϵ	6.4
phospholipase Cγ	(1HSQ)	NMR	Gln18N−Glu22Oϵ	7.5
Src	(1SRL)	NMR	Arg19N−Asp23Oδ	6.0

[a] Distances were obtained by RasMol (*35*). [b]Protein Data Bank accession number of the coordinate used to measure is indicated in parentheses.

acidic residue. Table 2 shows the distances between the two closest atoms corresponding to the N of Glu17 and the O_δ of Asp21 of PI3K SH3 in various SH3 domains. In most of SH3 domains, the distance is approximately 3 Å. This indicates that a similar hydrogen bond is generally formed. In contrast, the two atoms are at a distance of 6 Å or more in some SH3 domains such as Itk, phospholipase Cγ, and Src. Presence or absence of hydrogen-bonding is probably another mechanism to increase the diversity in structure and ligand specificity of SH3 domains. Using phage display libraries, Rickles et al. (*33*) showed that PI3K SH3 preferred the sequence RXXRPLPPLPPP, while Src SH3 selected XXXRPLPPLPXP. Since the residue at the fourth position is thought to make contact with the conserved acidic residue (*12, 34*), an Arg residue is selected by both of the domains. However, an Arg residue at the first position is selected only by PI3K SH3. Presence of a hydrogen-bond network and a resultant conformation of the RT loop may require the strict selection of the residue at the first position. They also showed that Fyn SH3 preferred the sequence XXXRPLPP(I/L)PXX where an Arg residue is not at the first position. This can be because a hydrogen-bond network of Fyn SH3 is weaker than that of PI3K SH3. Actually, the distance between Arg96N and Asp100O_δ of Fyn SH3 determined by NMR method is 4.9 Å (Table 2).

The effect of the D21N mutation is extended over the RT loop to the hydrophobic ligand binding cleft of the PI3K SH3 domain as shown in Figure 10A. Booker et al. (*11*) measured the ^{1}H chemical shift changes of PI3K SH3 induced by the binding of a 21-residue dynamin-derived synthetic peptide and determined 42 side-chain resonances of 15 residues as ligand-sensitive. These residues were Leu11, Tyr12, Tyr14, Glu17, Glu19, Asp21, Ile53, Gly54, Trp55, Leu56, Asp68, Pro70, Gly71, Tyr73, and Val74. Our results showed eight residues (nine residues when Tyr73 is included) out of them were affected by the D21N mutation. Therefore, the mutation of Asp21 causes structural deformation in more than half of the ligand-recognition site of the SH3 domain. For the role of the conserved acidic residue, it has been emphasized so far that the residue strengthens the ligand binding and determines the binding orientation (plus or minus) of a pseudosymmetric PxxP-containing peptide by ionic interactions with a basic residue positioned before or after the PxxP motif (*14*). Our results show that Asp21 of PI3K SH3 plays another important role of forming a proper and functional ligand binding cleft of the SH3 domain, which is necessary for specific intracellular signal transduction.

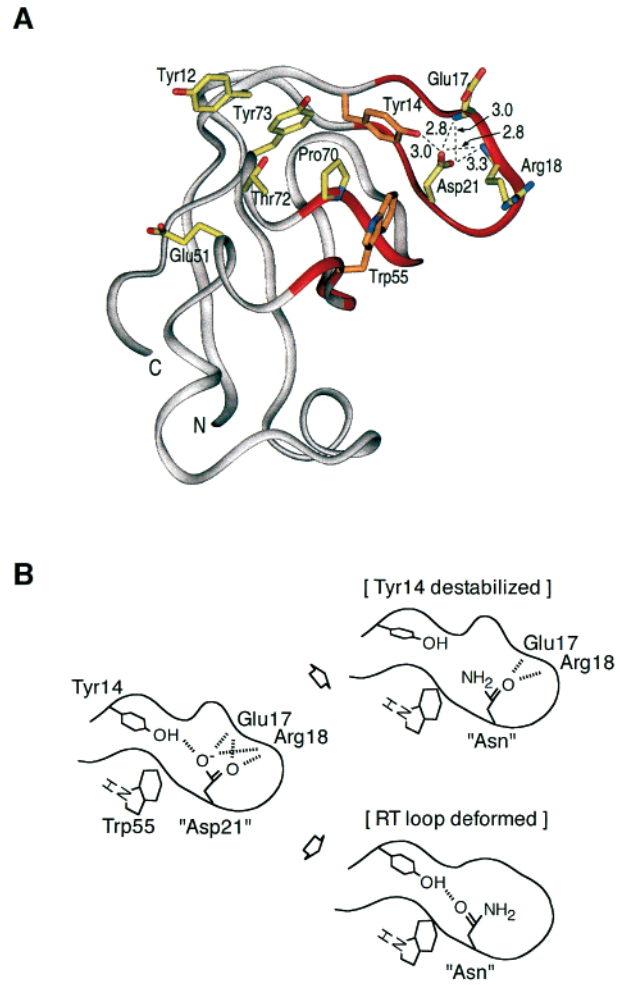

FIGURE 10: Effects of the D21N mutation on the PI3K SH3 structure. (A) C_α backbone trace of the PI3K SH3 structure depicting the side chains of residues that constitute the ligand binding cleft (Protein Data Bank accession number 1PKS) (*10*). The side chains and backbone amide nitrogen atoms of Glu17 and Arg18 were also drawn. The affected main chains (Lys15−Asp23, Gly54−Gly58 except Leu56, and Gly67−Pro70) and aromatic side chains (Tyr14 and Trp55) by the D21N mutation were colored in red and orange, respectively. Several selected distances relating with the O_δ atoms of Asp21 are shown in Å: Asp21$O_{\delta1}$−Glu17N, Asp21$O_{\delta1}$−Glu18N, Asp21$O_{\delta2}$−Tyr14O_η, Asp21$O_{\delta2}$−Glu17N, and Asp21$O_{\delta2}$−Arg18N. The figure was generated using InsightII (Molecular Simulations, San Diego, CA). (B) Models showing the effect of the D21N mutation on the structure of the RT loop of the PI3K SH3 domain. The D21N mutation may break an interaction between Asp21 and Tyr14 (Tyr14 destabilized) or disrupt an association between Asp21 and Glu17 or Arg18 (RT loop deformed).

ACKNOWLEDGMENT

We thank Masanori Osawa for affording us an opportunity to start the collaboration, Hideki Kusunoki for helpful discussions, and Noriko Suzuki for her help in preparing the resonance assignment tables.

SUPPORTING INFORMATION AVAILABLE

Tables 1 and 2 containing NMR chemical shifts of ^{1}H and ^{15}N resonances of the PI3K SH3 domain and its D21N mutant, respectively, and Table 3 showing several parameters used to determine the dissociation constants of the wild-type PI3K SH3 domain and its mutants for the RLP1 peptide. These materials are available free of charge via the Internet at http://pubs.acs.org.

REFERENCES

1. Mayer, B. J., Hamaguchi, M., and Hanafusa, H. (1988) *Nature 332*, 272−275.
2. Pawson, T. (1995) *Nature 373*, 573−580.
3. Kapeller, R., and Cantley, L. C. (1994) *BioEssays 16*, 565−576.
4. Vanhaesebroeck, B., and Waterfield, M. D. (1999) *Exp. Cell Res. 253*, 239−254.
5. Gout, I., Dhand, R., Hiles, I. D., Fry, M. J., Panayotou, G., Das, P., Truong, O., Totty, N. F., Hsuan, J., Booker, G. W., Campbell, I. D., and Waterfield, M. D. (1993) *Cell 75*, 25−36.
6. Barfod, E. T., Zheng, Y., Kuang, W.-J., Hart, M. J., Evans, T., Cerione, R. A., and Ashkenazi, A. (1993) *J. Biol. Chem. 268*, 26059−26062.
7. Harrison-Findik, D., Šuša, M., and Varticovski, L. (1995) *Oncogene 10*, 1385−1391.
8. Zhang, Q.-X., Davis, I. D., and Baldwin, G. S. (1996) *Biochim. Biophys. Acta 1312*, 207−214.
9. Harpur, A. G., Layton, M. J., Das, P., Bottomley, M. J., Panayotou, G., Driscoll, P. C., and Waterfield, M. D. (1999) *J. Biol. Chem. 274*, 12323−12332.
10. Koyama, S., Yu, H., Dalgarno, D. C., Shin, T. B., Zydowsky, L. D., and Schreiber, S. L. (1993) *Cell 72*, 945−952.
11. Booker, G. W., Gout, I., Downing, A. K., Driscoll, P. C., Boyd, J., Waterfield, M. D., and Campbell, I. D. (1993) *Cell 73*, 813−822.
12. Yu, H., Chen, J. K., Feng, S., Dalgarno, D. C., Brauer, A. W., and Schreiber, S. L. (1994) *Cell 76*, 933−945.
13. Liang, J., Chen, J. K., Schreiber, S. L., and Clardy, J. (1996) *J. Mol. Biol. 257*, 632−643.
14. Lee, C.-H., Cowburn, D., and Kuriyan, J. (1998) *Methods Mol. Biol. 84*, 3−31.
15. Borchert, T. V., Mathieu, M., Zeelen, J. P., Courtneidge, S. A., and Wierenga, R. K. (1994) *FEBS Lett. 341*, 79−85.
16. Musacchio, A., Saraste, M., and Wilmanns, M. (1994) *Nat. Struct. Biol. 1*, 546−551.
17. Okishio, N., Nagai, M., Fukuda, R., Nagatomo, S., and Kitagawa, T. (2000) *Biopolymers 57*, 208−217.
18. Gill, S. C., and von Hippel, P. H. (1989) *Anal. Biochem. 182*, 319−326.
19. Strickland, E. H. (1974) *CRC Crit. Rev. Biochem. 2*, 113−175.
20. Renzoni, D. A., Pugh, D. J. R., Siligardi, G., Das, P., Morton, C. J., Rossi, C., Waterfield, M. D., Campbell, I. D., and Ladbury, J. E. (1996) *Biochemistry 35*, 15646−15653.
21. Delaglio, F., Grzesiek, S., Vuister, G. W., Zhu, G., Pfeifer, J., and Bax, A. (1995) *J. Biomol. NMR 6*, 277−293.
22. Garrett, D. S., Powers, R., Gronenborn, A. M., and Clore, G. M. (1991) *J. Magn. Reson. 95*, 214−220.
23. Mattiello, D. L., Warren, W. S., Mueller, L., and Farmer, B. T., II. (1996) *J. Am. Chem. Soc. 118*, 3253−3261.
24. Jeener, J., Meier, B. H., Bachmann, P., and Ernst, R. R. (1979). *J. Chem. Phys. 71*, 4546−4553.
25. Kay, L. E., Keifer, P., and Saarinen, T. (1992) *J. Am. Chem. Soc. 114*, 10663−10665.
26. Zhang, O., Kay, L. E., Olivier, J. P., and Forman-Kay, J. D. (1994) *J. Biomol. NMR 4*, 845−858.
27. Farrow, N. A., Muhandiram, R., Singer, A. U., Pascal, S. M., Kay, C. M., Gish, G., Shoelson, S. E., Pawson, T., Forman-Kay, J. D., and Kay, L. E. (1994) *Biochemistry 33*, 5984−6003.
28. Woody, R. W. (1995) *Methods Enzymol. 246*, 34−71.
29. Kelly, S. M., and Price, N. C. (1997) *Biochim. Biophys. Acta 1338*, 161−185.
30. Koyama, S., Yu, H., Dalgarno, D. C., Shin, T. B., Zydowsky, L. D., and Schreiber S. L. (1993) *FEBS Lett. 324*, 93−98.
31. Mongioví, A. M., Romano, P. R., Panni, S., Mendoza, M., Wong, W. T., Musacchio, A., Cesareni, G., and Di Fiore, P. P. (1999) *EMBO J. 18*, 5300−5309.

32. Arold, S., O'Brien, R., Franken, P., Strub, M.-P., Hoh, F., Dumas, C., and Ladbury, J. E. (1998) *Biochemistry 37*, 14683−14691.
33. Rickles, R. J., Botfield, M. C., Weng, Z., Taylor, J. A., Green, O. M., Brugge, J. S., and Zoller, M. J. (1994) *EMBO J. 13*, 5598−5604.
34. Feng, S., Chen, J. K., Yu, H., Simon, J. A., and Schreiber, S. L. (1994) *Science 266*, 1241−1247.
35. Sayle, R. A., and Milner-White, E. J. (1995) *Trends Biochem. Sci. 20*, 374−376.

BI001607V